

A possible cause of decreasing summer rainfall in northeast Australia

Jianping Li,^{a*} Juan Feng^{a,b} and Yun Li^c

^a State Key Laboratory of Numerical Modeling for Atmospheric Sciences and Geophysical Fluid Dynamics, Institute of Atmospheric Physics, Chinese Academy of Sciences, Beijing, China

^b College of Atmospheric Sciences, Lanzhou University, Lanzhou, Gansu, China

^c CSIRO Mathematical and Information Sciences, CSIRO Water for a Healthy Country Flagship, Wembley, Western Australia, Australia

ABSTRACT: The NCEP/NCAR reanalysis and precipitation data from the Australian Bureau of Meteorology are used to analyse variability in rainfall during the austral summer (December–March, DJFM) in northeast Australia (NEA). NEA rainfall shows a marked decrease over the past 50 years, mainly in the austral summer. Our analysis reveals that the summer rainfall decrease in NEA is generally an interdecadal phenomenon. The declining trend has an imprint in the tropical Australian summer monsoon (TASM). Not only does TASM have a phase-to-phase influence on NEA summer rainfall at the interannual scale, it is also closely linked with interdecadal variation in NEA summer rainfall. Thus, the decrease in NEA at the interdecadal scale could be attributed to corresponding variation in TASM. Moreover, the coupled linkage between TASM and NEA summer rainfall appears to be largely independent of El Niño–Southern Oscillation. One possible reason for the interdecadal weakening trend in TASM is a sustained interdecadal warming trend in sea surface temperature (SST) over the Wharton Basin (100°–130°E, 20°–5°S). When the Wharton Basin is in a cold state, anomalous westerlies occur in the lower troposphere in the TASM region, and cyclonic circulation anomalies and rising flows occur in the low and middle troposphere over NEA, which are associated with a strong TASM situation, consequently favouring enhanced rainfall over NEA; the opposite occurs in the case of a warm Wharton Basin. SST over the Wharton Basin has shown a continuous warming trend over the past 60 years, contributing to the weakening of TASM and, consequently, a decrease in NEA summer rainfall. Copyright © 2011 Royal Meteorological Society

KEY WORDS tropical Australian summer monsoon; northeast Australian summer rainfall; ENSO

Received 15 February 2009; Revised 10 January 2011; Accepted 22 February 2011

1. Introduction

Australian rainfall shows a high degree of variability (e.g. Drosdowsky, 1993; Smith *et al.*, 2000). The rainfall pattern is important for agriculture and for managing water resources. Thus, a better understanding of the causes of precipitation variability is necessary to avoid financial losses in the Australian economy. As northeast Australia (NEA) has a large population and a vibrant economy, variability in rainfall over NEA has a strong influence on economic growth and daily life in this region.

The annual rainfall amount over Australia has changed significantly in recent decades: rainfall has declined in NEA, southeast Australia, and southwest Western Australia (SWWA), but has shown a marked increase over north Western Australia (NWA). The rainfall decrease in SWWA has been studied intensely in recent years (e.g. Smith *et al.*, 2000; Cai and Watterson, 2002; IOCI, 2002; Pitman *et al.*, 2004; Cai *et al.*, 2005; Li *et al.*, 2005; Cai

and Cowan, 2006; Hope *et al.*, 2006; Meneghini *et al.*, 2007; Feng *et al.*, 2010a, 2010b), as has the increasing trend in NWA (Wardle and Smith, 2004; Rotstayn *et al.*, 2006; Shi *et al.*, 2008a, 2008b; Taschetto and England, 2008). In contrast, relatively little is known of the cause and mechanism of the decreased NEA rainfall. As noted by Nicholls (2006), an immediate priority for future detection and attribution studies would be the decline in rainfall along the east coast and in areas stretching inland from the coast.

Two recent papers have shed some light on this topic. Shi *et al.* (2008a) reported an anomalously high sea level pressure (SLP) over much of the Australian continent; the anticyclone circulation pattern is associated with southeasterly flows in NEA, resulting in variable rainfall east of 130°E and anomalously low rainfall to the west. However, the Australian anticyclone is located over southern Australia (south of 25°S) in austral summer; the region north of 25°S in Australia is strongly influenced by easterlies. This observation could not explain the reduced rainfall in NEA during the austral summer. Taschetto and England (2008) reported that the frequency of summertime extreme rainfall events in NEA has declined. However, the prescribed rainfall changes over

* Correspondence to: Jianping Li, State Key Laboratory of Numerical Modeling for Atmospheric Sciences and Geophysical Fluid Dynamics, Institute of Atmospheric Physics, Chinese Academy of Sciences, Beijing, China. E-mail: ljp@lasg.iap.ac.cn

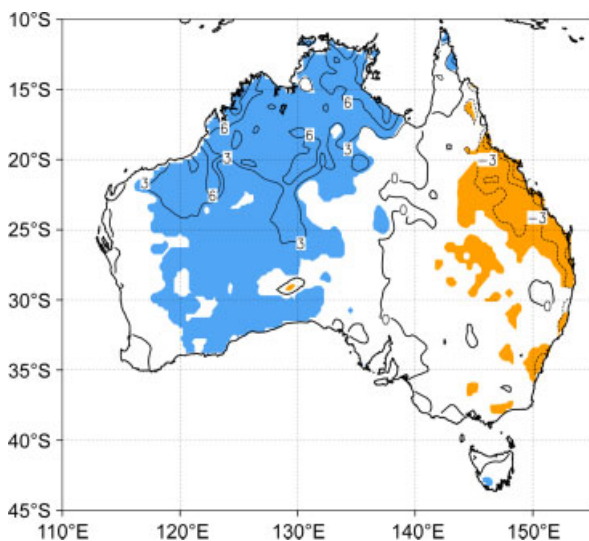


Figure 1. Summer (DJFM) rainfall trend based on Australian rainfall data over the period 1948–2007. The shaded areas indicate statistically significant trends at the 0.05 level (unit: mm/year). This figure is available in colour online at wileyonlinelibrary.com/journal/joc

NEA (Figure 1) are much larger than could be explained solely by extreme events; thus, the cause of the rainfall decrease over NEA remains an open question.

On the other hand, many studies have examined the relationship between El Niño–Southern Oscillation (ENSO) and Australian rainfall. The influence of sea surface temperature (SST) in the central and eastern Pacific on Australian rainfall variability has been clearly established (e.g. McBride and Nicholls, 1983; Drosdowsky and Williams, 1991; Lau and Nath, 1996; Murphy, 2004). Previous studies have provided evidence that warm El Niño events are generally accompanied by drought conditions over northern and eastern Australia, whereas above-average rainfall occurs during La Niña events. However, Power *et al.* (1999) indicated that the relationship between ENSO and rainfall anomalies averaged over Australia has collapsed. In addition, Cai *et al.* (2001) reported that the relation between NEA rainfall and ENSO fluctuates in tandem with annual rainfall anomalies, and that NEA rainfall shows a strong interdecadal variation along with intense interannual fluctuations. In fact, ENSO has a statistically significant influence on NEA summer rainfall over the period 1948–1976, but not after 1976 (the correlation coefficient between Niño3.4 index and NEA summer rainfall for 1948–1976 is -0.59 , significant at the 0.05 level; the correlation coefficient for 1977–2006 is -0.33 , which is not significant at the 0.05 level. Cai *et al.* (2010) proposed that the impacts of ENSO on southeast Queensland are asymmetry, and the influence is only significant in its negative events. However, there is a complete breakdown in the teleconnection with La Niña over southeast Queensland, contributing to the rainfall reduction. In this case, the cause of decrease in summer rainfall over NEA remains unknown, meaning that further research is required.

The influence of Indian Ocean SST anomalies on Australian rainfall has been studied in recent years (e.g. Nicholls, 1989; Simmonds, 1990; Ashok *et al.*, 2003; Murphy, 2004; Cai *et al.*, 2009). Nicholls *et al.* (1996) described an apparent change in the relationship between ENSO and Australian rainfall and temperature. The authors ascribed the change to an increase in Indian Ocean SST, and pointed out that interannual rainfall variability is amplified in regions affected by ENSO (Nicholls 1988), such as NEA. NEA is located at the margin of monsoon-affected Australia; consequently, rainfall variability in this region is affected by atmospheric phenomena rather than by ENSO (Murphy, 2004). However, few studies have discussed the relationship between the tropical Australian summer monsoon (TASM) and NEA rainfall.

In the present study, we explore both temporal variations in TASM and its influence on NEA summer rainfall variability. It is found that TASM strength has a statistically significant positive influence on NEA summer rainfall, and TASM itself shows strong interannual and interdecadal variability within an overall weakening trend, which is consistent with the decline in summer rainfall within NEA. The remainder of the paper is organized as follows. The dataset, methodology and model used in this study are described in Section 2. In Section 3, we focus on the relationship between TASM and Australian rainfall. A possible cause of the weakened trend in TASM is considered in Section 4. Finally, the conclusions and discussions are presented in Section 5.

2. Data, methodology and model

2.1. Data

The primary dataset used in this study is from the National Centers for Environmental Prediction/National Center for Atmospheric Research (NCEP/NCAR) reanalysis (Kalnay *et al.*, 1996), obtained from <http://www.cdc.noaa.gov/PublicData/>. Rainfall data were provided by the National Climate Centre (NCC) of the Australian Bureau of Meteorology, consisting of data on a $0.25^\circ \times 0.25^\circ$ grid. The SST data are the Improved Extended Reconstruction SST (IERSST; Smith and Reynolds, 2004) on a $2^\circ \times 2^\circ$ grid. The Niño3.4 index is from <http://www.cpc.noaa.gov/data/indices/> and is one of several ENSO indicators based on SST anomalies in the region of $(5^\circ\text{S}–5^\circ\text{N}, 170^\circ–120^\circ\text{W})$.

2.2. Methodology

A unified dynamical normalized seasonality (DNS) monsoon index, as introduced by Li and Zeng (2000, 2002, 2003), is applied to determine the magnitude and variability of TASM. This index is based on the intensity of seasonality of the wind fields, and can be used to depict the seasonal cycle and interannual variability of monsoon over various areas (Li and Zeng, 2005; Feng and Li, 2009; Feng *et al.*, 2010a; Zhang *et al.*, 2010). For a

given pressure level and grid point(i, j), the DNS index in the m -th month of the n -th year is given by

$$\delta_{nm}(i, j) = \frac{||\bar{\mathbf{V}}_W(i, j) - \mathbf{V}_{nm}(i, j)||}{||\bar{\mathbf{V}}(i, j)||} - 2,$$

where $\bar{\mathbf{V}}_W$ is the climatological winter wind vector as the reference state (here, averaged from 1968 to 1996), \mathbf{V}_{nm} is the wind vector in the m -th month of the n -th year, and $\bar{\mathbf{V}} = (\bar{\mathbf{V}}_W + \bar{\mathbf{V}}_S)/2$ is the climatological mean wind vector, where $\bar{\mathbf{V}}_S$ is the climatological summer wind (for the Northern Hemisphere, taking $\bar{\mathbf{V}}_W = \bar{\mathbf{V}}_{\text{Jan}}$ and $\bar{\mathbf{V}}_S = \bar{\mathbf{V}}_{\text{Jul}}$; for the Southern Hemisphere, taking $\bar{\mathbf{V}}_W = \bar{\mathbf{V}}_{\text{Jul}}$ and $\bar{\mathbf{V}}_S = \bar{\mathbf{V}}_{\text{Jan}}$). The norm $||A||$ is defined as $||A|| = (\int_S |A|^2 dS)^{1/2}$ where S denotes the domain of integration. At a given grid point(i, j),

$$||A_{i,j}|| \approx \Delta s \left[(|A_{i-1,j}^2| + 4|A_{i,j}^2| + |A_{i+1,j}^2|) \cos \varphi_j + |A_{i,j-1}^2| \cos \varphi_{j-1} + |A_{i,j+1}^2| \cos \varphi_{j+1} \right]^{1/2}$$

where φ_j is the latitude at point (i, j) and $\Delta s = a\Delta\varphi\Delta\lambda/4$, a is the mean radius of the Earth, and $\Delta\varphi$ and $\Delta\lambda$ (in radians) are the resolution in the meridional and zonal directions, respectively. A value of 2 is subtracted in the right-hand side of the formula, because it is the critical value of significance of the quantity. The case when $\delta_{nm}(i, j) > 0$ means that the prevailing winds direction shifts by at least 90° between winter and summer (Li and Zeng, 2000).

A large-scale monsoon index MI_{nm} in the m -th month of the n -th year is defined as a measure of the averaged DNS over a monsoon domain, given by

$$MI_{nm} = \{\delta_{nm}(i, j)\},$$

where the symbol $\{\bullet\}$ denotes the areal average of δ within a chosen monsoon domain at a certain pressure level (generally 850 or 925 hPa). For details on the physical definition see Li and Zeng (2000, 2002). Following Li and Zeng (2002), the region (20° – 5° S, 100° – 160° E) is selected as the TASM domain and 925 hPa is selected as the level of the monsoon index with which to construct the TASM index (TASMI).

Taking into account the fact that the Intertropical Convergence Zone (ITCZ) frequently appears as a convective belt in the tropics, the zonal component of wind at 850 hPa is usually larger than the meridional component; thus, to a good approximation, a vortex can be calculated from the meridional shear of the zonal wind component. Therefore, the averaged position of the ITCZ is defined as the location where the vortex reaches its maximum value (Wei *et al.*, 2008).

The relation between TASM and NEA summer rainfall is investigated by correlation, composite and partial correlation analyses. Here, the composite analyses for an index are the differences between the strong (greater than $+1$ standard deviation of the index) and weak values (less

than -1 standard deviation of the index). In addition, considering that NEA summer rainfall shows strong interdecadal variation (Cai *et al.*, 2001; Figure 2(b)), we separated the variation into two parts by applying a 7-year Gaussian filter to the original data, in order to analyse the influence of TASM on NEA summer rainfall at different time scales. The high-pass part is considered to be variation on the interannual scale, while the low-pass part is taken as variation on the interdecadal scale. By taking into account the effect of filtering on the degrees of freedom and by employing a significance test, the effective degrees of freedom are readily evaluated.

Davis (1976) and Chen (1982) presented a method for estimating the effective degrees of freedom N , as $N = n/T$, whereby

$$T = \sum_{\tau=0}^K C_{xx}(\tau) C_{yy}(\tau),$$

where $C_{xx}(\tau)$ and $C_{yy}(\tau)$ are the autocorrelation coefficients of x_i ($i = 1, \dots, n$) and y_i ($i = 1, \dots, n$), respectively, with a lagged scale τ . The maximum of the integer K corresponds to $n/2$.

2.3. Model

The atmospheric general circulation model used in this study is the NCAR Community Atmospheric Model version 3 (CAM3). The horizontal resolution is T42 (approximately $2.8^\circ \times 2.8^\circ$), with 26 hybrid vertical levels. (A complete description of this model is available online through <http://www.ccsm.ucar.edu/models/atm-cam/docs/description/>).

3. Relationship between TASM and NEA rainfall

3.1. Selection of the analysis period

Northern Australia experiences a tropical climate with a distinct rainy season that typically begins during November and ends in April. Much of the area receives more than 75% of its annual mean rainfall during these 6 months (Ropelewski and Halpert, 1987; Ropelewski, 1989). Previous studies have suggested that the rainfall decrease in NEA is mainly a summer phenomenon (Nicholls, 2006), and trends in half-year rainfall over the period 1952–2002 dominate the trends in annual rainfall over the full period of 1901–2002 (Smith, 2004). Accordingly, the present analysis focuses on the summer period in the second half of the twentieth century.

In previous studies, the months December, January, and February (DJF) are generally defined as the summer period (e.g. Frederiksen *et al.*, 1999; Hendon *et al.*, 2007). To demonstrate the decreasing rainfall trend completely and exactly, trends were assessed monthly. The results indicate that NEA rainfall in March shows a similar trend to that in December–February, being as extensive as that in January. Thus, the period December–March (DJFM) is taken as the analysis period.

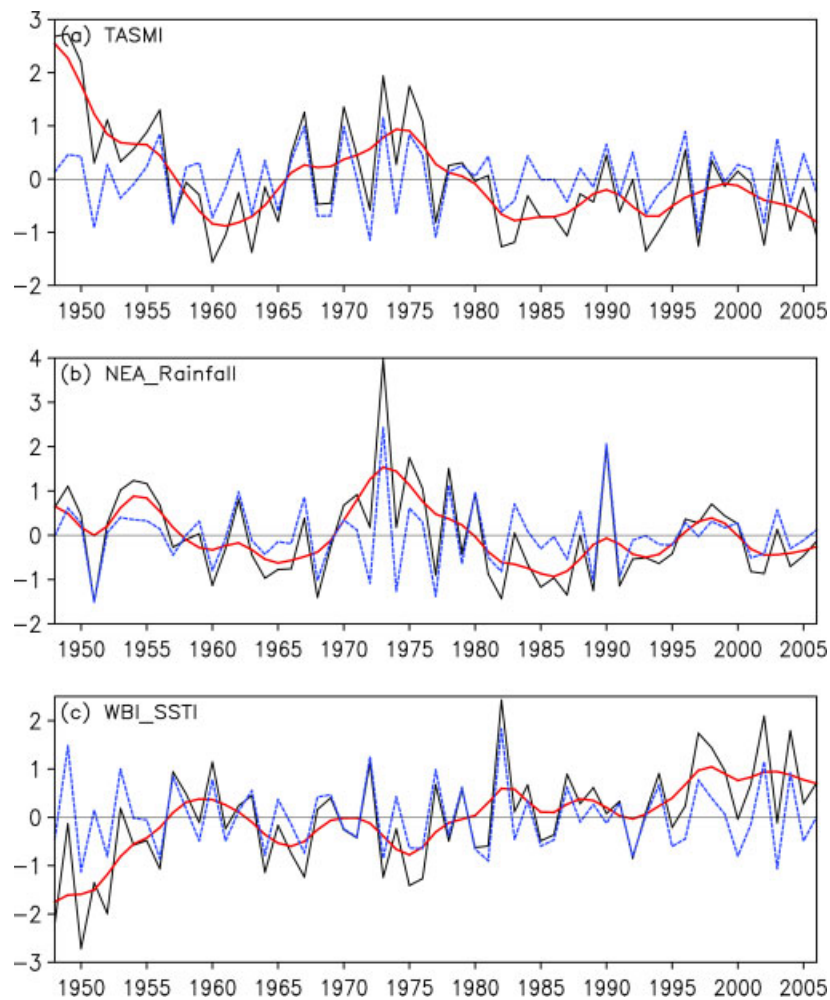


Figure 2. (a) Normalized time series of TASMI (solid line). The thick solid (dashed) lines indicate the interdecadal (interannual) variation filtered by a 7-year Gaussian filter. (b) As for (a), but for the NEA summer rainfall series. (c) As for (a), but for WB-SSTI, which is the areal-averaged SST over the Wharton Basin (100° – 130° E, 20° – 5° S). This figure is available in colour online at wileyonlinelibrary.com/journal/joc

Figure 1 shows the DJFM rainfall trend in Australia during recent decades. Overall, the spatial pattern of the precipitation trend can be separated into two main parts: being positive in Western Australia and negative in eastern Australia. The area with the largest negative value is located along the coast of NEA; the negative values decrease toward inland areas. The dividing line between the positive and negative trends is located at approximately 140° E.

3.2. Relationship between TASMI and NEA summer rainfall

Figure 2(a) shows the normalized time series of TASMI for the past 60 years. TASMI shows strong interannual and interdecadal variability along with a clear long-term decreasing trend. TASMI was in a positive phase from 1948 to 1956, a negative phase between 1957 and 1966, a positive phase from 1967 until the end of the 1970s, and a negative phase from the 1980s until the present. The amplitude of TASMI has weakened during this time. If a strong (weak) TASMI year is taken as a year with TASMI greater (less) than ± 1 standard deviation of the index, we find that since the mid-1970s, there have

been no years with a strong summer monsoon, and years with a weak summer monsoon have become increasingly frequent.

TASMI is generally closely linked with NEA summer rainfall (Figure 2(a), (b)), as indicated by a correlation coefficient of 0.64 obtained between TASMI and summer rainfall averaged over NEA, east of 140° E and north of 25° S (Table I). NEA summer rainfall shows a decreasing trend that is well in phase with TASMI. Noting that, TASMI does not show significant trend for the sub-periods pre- and post-1980, accordingly, there is no clear trend in NEA summer rainfall (Cai *et al.*, 2010).

Figure 3 shows a correlation map between TASMI and Australian summer rainfall. Figure 3(a) shows that TASMI is significantly positively correlated with summer rainfall over NEA, indicating that stronger TASMI favours larger amounts of summer rainfall in NEA, and vice versa. Furthermore, the correlation coefficient between TASMI and NEA summer rainfall is 0.65 for the interannual time scale and 0.68 for the interdecadal time scale (Table I). Thus, it could be concluded that TASMI is responsible for both interannual and interdecadal variations in NEA summer rainfall: when TASMI

Table I. Correlation coefficients between tropical Australian summer monsoon index (TASMI) and various indices.

	NEA-R ^a	ITCZL_NEA ^b	U-shearing ^c	Vapour ^d	WB-SSTI ^e
Raw series	0.64 ⁱ	-0.63 ⁱ	0.84 ⁱ	0.65 ⁱ	-0.71 ⁱ
Interannual ^f	0.65 ⁱ	-0.71 ⁱ	0.81 ⁱ	0.64 ⁱ	-0.66 ⁱ
Interdecadal ^g	0.68 ^h	-0.61 ^h	0.88 ⁱ	0.73 ^h	-0.81 ^h
Removal Niño3.4	0.52 ^h	-0.55 ⁱ	0.78 ⁱ	0.50 ⁱ	-0.63 ⁱ

^a NEA-R is the areal-averaged austral summer rainfall over the NEA region.

^b ITCZL_NEA is the mean latitude position of the ITCZ over NEA within 140°–160°E.

^c The U-shearing index is the zonal wind meridional shearing, defined as the difference in zonal wind at 850 hPa between 10° and 25°S, within 130°–160°E.

^d The Vapour index indicates vapour transport at 925 hPa within the region (140°–160°E, 25°–10°S).

^e WB-SSTI is the areal-averaged SST over the Wharton Basin (100°–130°E, 20°–5°S).

^f Interannual represents variations at scales less than 7 years.

^g Interdecadal represents variations at scales beyond 7 years.

^h Statistically significant correlations at the 0.05 level.

ⁱ Statistically significant correlations at the 0.01 level.

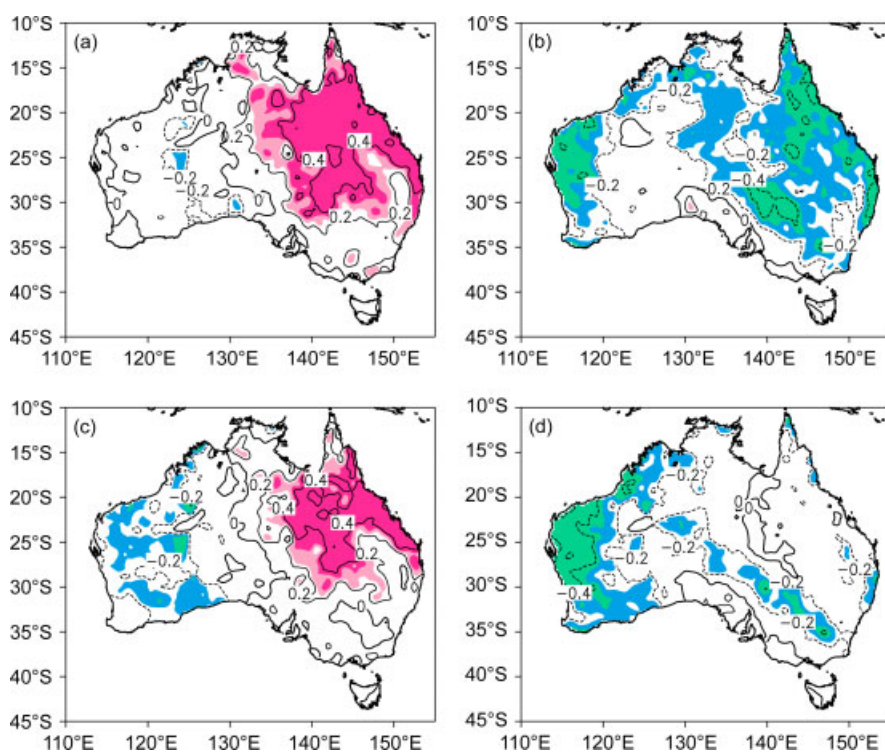


Figure 3. Correlation maps between Australian summer rainfall and (a) TASMI and (b) the Niño 3.4 index. (c) As for (a), but after removing the effect of ENSO. (d) As for (b), but after removing the effect of TASMI. The shading indicates a statistically significant correlation at the 0.05 level. This figure is available in colour online at wileyonlinelibrary.com/journal/joc

is strong (weak), there occurs more (less) summer rainfall in NEA.

Here, we consider the circulation anomalies associated with TASMI. Figure 4 shows composite differences in selected variables between the strong and weak index polarities of TASMI. There are distinct differences in lower tropospheric circulation between strong and weak TASMI years. In strong TASMI years (Figure 4(a)) very strong westerly anomalies are observed over the tropical Australian monsoon region, resulting in enhanced strength of cyclonic vorticity over NEA and the adjacent ocean to the east. The point could be verified from the very strong correlation (with coefficient of 0.84;

Table I) between TASMI and the meridional shear of the zonal wind index, which is defined as the difference in zonal wind at 850 hPa between 10° and 25°S, within 130°–160°E. Thus, a significant negative SLP anomaly lies over Australia and the adjacent ocean. This pattern acts to intensify the Australian cyclone located over northern Australia during summer, and NEA is covered by an anomaly pattern comprising a strong cyclonic circulation. Moreover, vapour transportation in the lower troposphere over the NEA region (140°–160°E, 25°–10°S) is strongly correlated with TASMI (correlation coefficient = 0.65; Table I), indicating that the strengthened westerlies bring more vapour to the NEA region. The

mean position of the ITCZ over NEA (ITCZ_NEA, averaged over 140°–160°E) is closely associated with TASM (correlation coefficient = −0.63; Table I); i.e. ITCZ_NEA is located southward in years with strong TASM (Figure 4(b)), indicating that the deep convection center moves southward. The strengthened cyclonic vorticity and southward shift of the ITCZ_NEA favour anomalous rising flows over NEA (Figure 4(c)), associated with enhanced rainfall over NEA.

Figure 5 shows a time series of the averaged latitudes of ITCZ_NEA, cyclonic vorticity, and vapour transportation at 925 hPa. The weak situation of TASM (Figure 3(a)) over the past 30 years is accompanied by a northward shift in ITCZ_NEA (Figure 5(a)), subdued cyclonic vorticity (Figure 5(b)), and reduced vapour transport over NEA (Figure 5(c)), together resulting in reduced NEA summer rainfall.

The above results show that variations in NEA summer rainfall are linked with variations in TASM. In contrast, previous studies have suggested that summer rainfall in eastern Australia is affected by ENSO (Figure 3(b)). Moreover, TASM is correlated with ENSO (correlation

coefficient between TASMI and Niño3.4 index = −0.53). Thus, the question of whether the relation between TASM and NEA rainfall is influenced by ENSO warrants further consideration. Here, we use partial correlation to assess whether the relationship between TASM and NEA summer rainfall is independent of ENSO. The partial correlations between TASMI and summer rainfall, after removing ENSO effects, show a similar pattern to the total correlations (compare Figure 3(c) with (a)). The strong correlation over NEA is barely weakened after removing the effects of ENSO, indicating that the TASM–NEA rainfall relationship is linearly independent of ENSO. In contrast, the significant correlation between the Niño3.4 index and NEA rainfall is no longer seen once the effect of TASM has been removed (compare Figure 3(d) with (b)). Noting that the relationship between TASM and NEA rainfall is reduced after removing the effects of ENSO (compare Figure 3(d) with (b)), indicating ENSO has an influence on NEA summer rainfall, i.e. a non-linear influence (Cai *et al.*, 2010). Furthermore, the relations between TASMI and each of ITCZ_NEA locations, vapour transport, zonal wind meridional shearing, and cyclonic vorticity indices are barely weakened (all remain significant at the 0.01 level) after removing the effect of ENSO (Table I). This result reveals that the TASM–NEA summer rainfall relationship is largely linearly independent of the influence of ENSO. However, this does not necessarily indicate that we can separate the contributions of ENSO and TASM to variations in summertime rainfall over NEA.

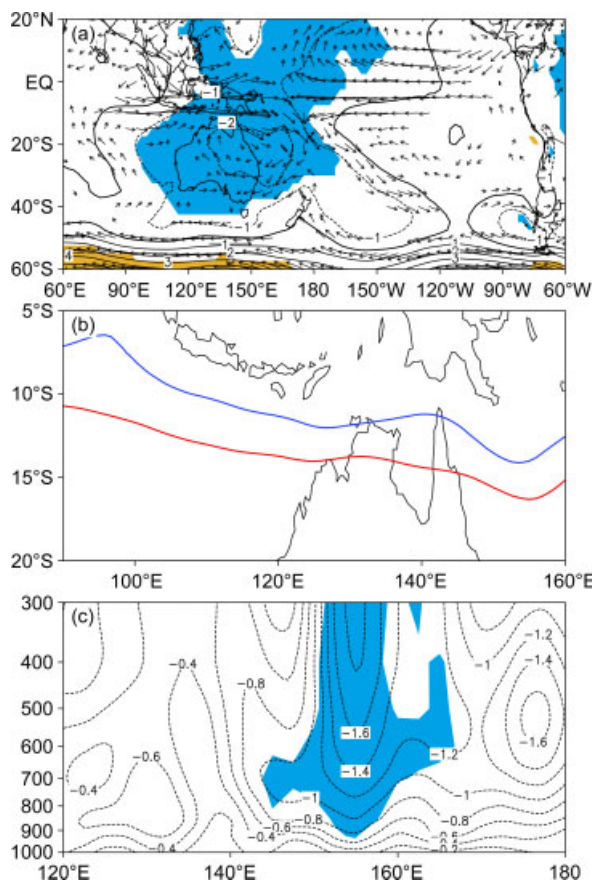


Figure 4. (a) Composite differences in 850 hPa wind (vectors) and SLP (contours) between strong and weak TASM years during DJFM. For the wind vectors, only those values significant at the 0.05 level are shown. The contour interval is 1 hPa. Shaded areas indicate a statistically significant SLP difference at the 0.05 level. (b) Position of the ITCZ during strong (red) and weak (blue) TASM years. (c) As for (a), but for the vertical velocity averaged over 25°–5°S (unit: P/s). This figure is available in colour online at wileyonlinelibrary.com/journal/joc

4. Why does TASM experience a weakening trend?

Hereinbefore, we reported that variations in summer rainfall over NEA are closely linked with TASM strength. In this case, why does TASM show a subdued trend, and what external forcing is responsible for its weakening?

Figure 6(a) shows the composite differences in SST between strong and weak TASM years. The composite pattern mainly indicates an ENSO-induced mode, with significant negative anomalies over the middle and eastern tropical Pacific. There also exists a significant negative anomaly pattern over the tropical Indian Ocean and the Indian Ocean westward of Western Australia (especially the Wharton Basin). However, in recalculating the composite analysis of strong minus weak TASM years after excluding years with high and low polarities of ENSO (i.e. focusing on non-ENSO years), as shown in Figure 6(b), the significant signal over the tropical Pacific has largely disappeared and the signal over the tropical Indian Ocean has become much weaker, whereas the significant signal over the Wharton Basin is not only still there but also becomes stronger. This result indicates that SST in the Wharton Basin may play an important role in controlling variations in TASM.

To further show how TASM is linked to SST in the Wharton Basin, an SST index, WB-SSTI, is defined as the areal averaged SST over the Wharton Basin (100°–130°E, 20°–5°S). WB-SSTI is strongly correlated

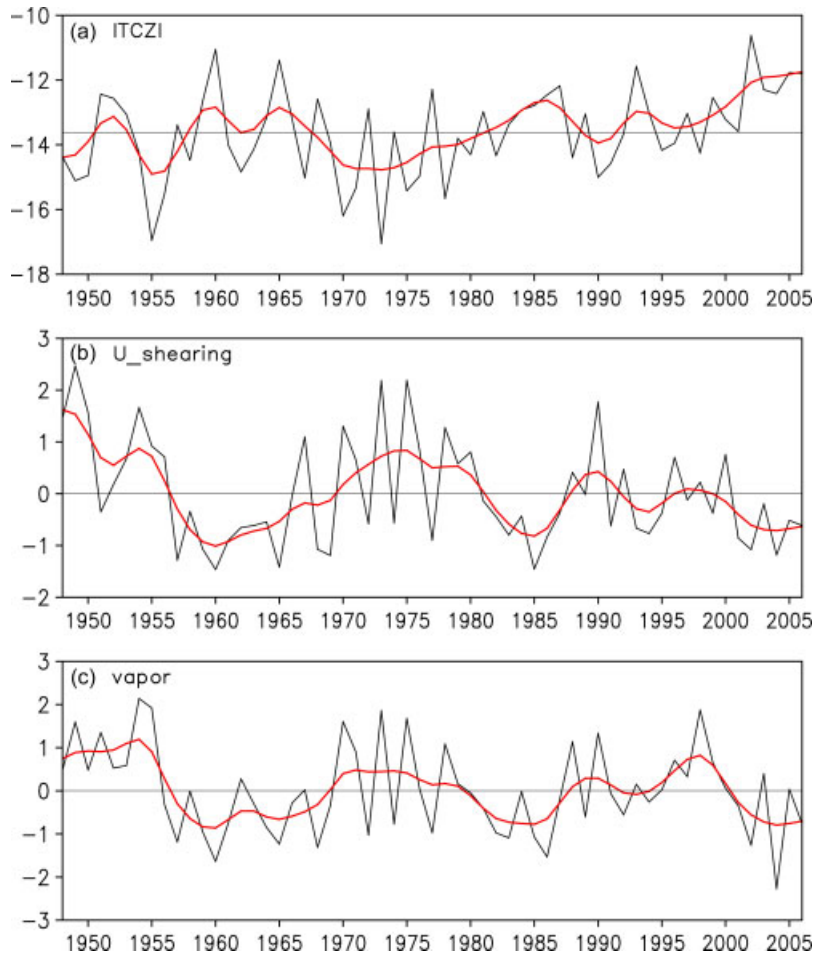


Figure 5. (a) Mean latitude position ($^{\circ}$ S) of the ITCZ over NEA within 140° – 160° E. (b) Normalized time series of the zonal wind meridional shearing index, which is defined as the difference in zonal wind at 850 hPa between 10° S and 25° S, within 130° – 160° E. (c) Normalized time series of vapour transport at 925 hPa within the region (140° – 160° E, 25° – 10° S). Thick solid lines indicate the interdecadal variation filtered by a 7-year Gaussian filter. This figure is available in colour online at wileyonlinelibrary.com/journal/joc

with TASMI at both interannual (correlation coefficient of -0.66) and interdecadal (correlation coefficient of -0.81) scales (Figure 2(c) and Table I). Moreover, the correlation between TASMI and WB-SSTI shows little change after removing the effects of ENSO (it changes from -0.71 to -0.63 , with both values being significant at the 0.01 level), suggesting their linkage is not strongly contaminated by ENSO.

To investigate possible dynamical linkages between TASMI and Wharton Basin SST, Figure 7 shows the composite differences between cold and warm WB-SSTI years in terms of winds and geopotential in the lower troposphere at 850 hPa, large-scale moist static stability, vertical shear of zonal wind, and vertical circulation, revealing significant differences. The circulation pattern in Figure 7(a) is similar to that in Figure 4(a). That is, during colder SST years in the Wharton Basin, strong westerly anomalies occur over the tropical Australian monsoon region, and positive anomalies in large-scale moist static stability (Figure 7(b)) – defined by the vertical difference between 500 and 850 hPa pseudoequivalent potential temperature (θ_{se}) – are observed over the region; consequently, the rising flow over the Wharton

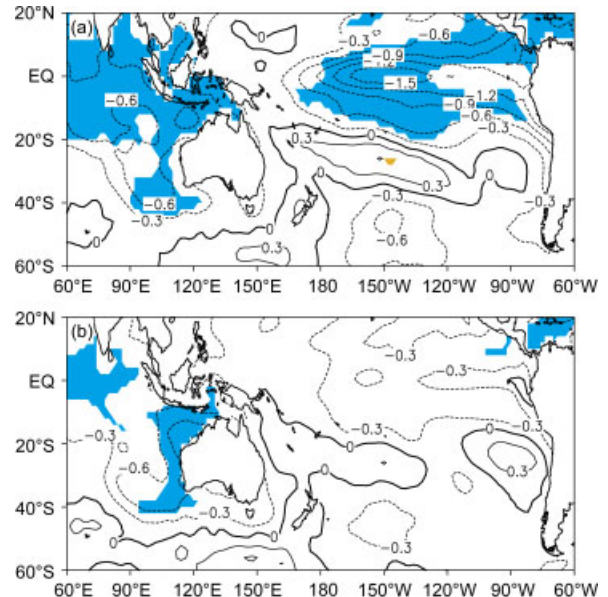


Figure 6. (a) Composite difference in SST between strong and weak TASMI years. (b) As for (a), but for non-ENSO years. Shading indicates statistically significant difference at the 0.01 level. This figure is available in colour online at wileyonlinelibrary.com/journal/joc

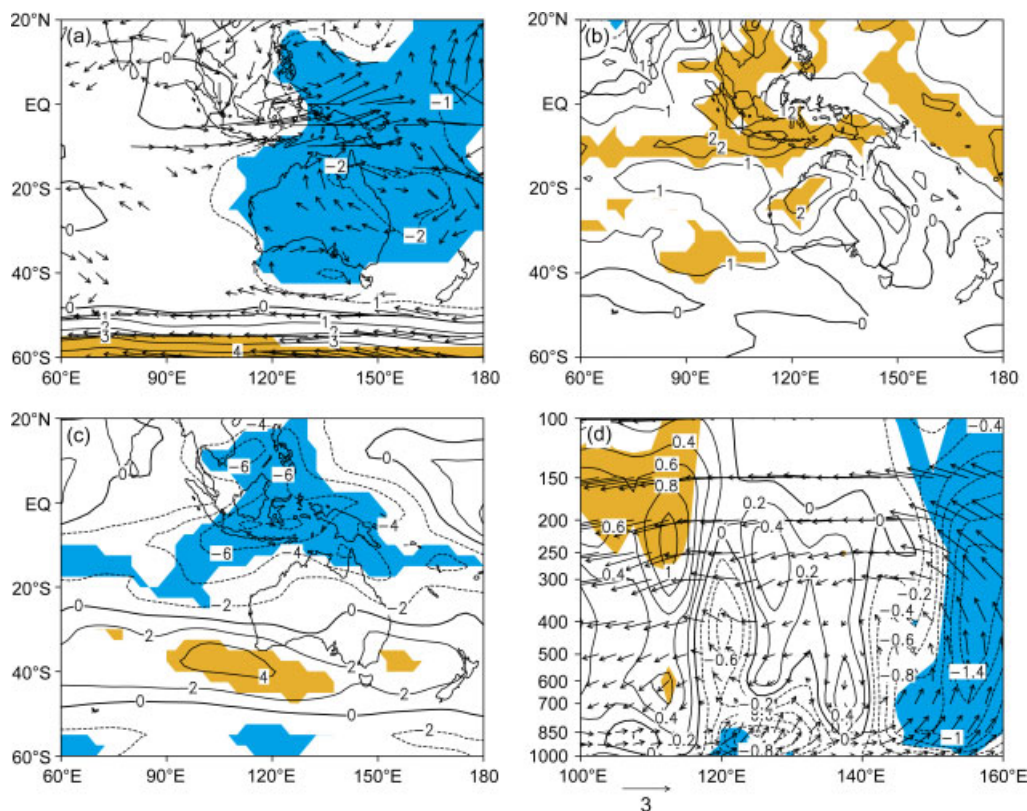


Figure 7. Composite differences between cold and warm WB-SSTI years. (a) SLP (contours) and wind (vectors) at 850 hPa (units: hPa for SLP, m/s for wind). (b) Vertical difference between the 500 and 850 hPa pseudoequivalent potential temperature (θ_{se}) (unit: K). (c) Vertical shear of the zonal wind between 200 and 850 hPa (unit: m/s). (d) Zonal vertical circulation (vectors) and vertical velocity (contours) (unit: P/s). Shading indicates statistically significant difference at the 0.05 level. This figure is available in colour online at wileyonlinelibrary.com/journal/joc

Basin is restrained and anomalous sinking flow is induced (Figure 7(d)), corresponding to the anticyclonic anomaly circulation pattern over the region.

Strong negative anomalies in vertical shear of the zonal wind between the upper (200 hPa) and lower troposphere (850 hPa) occur over the tropical Australian monsoon region (Figure 7(c)), which acts to intensify the zonal anti-clockwise vertical circulation over the region (Figure 7(d)) and rising motion in the east. The strong negative anomalies in vertical shear of the zonal wind, which correspond to cold SST anomalies in the Wharton Basin, could be further estimated from the significant correlation between WB-SSTI and the zonal wind vertical shear index between the upper and lower levels in the region (120° – 160° E, 15° – 5° S). Therefore, the cold SST anomalies in the Wharton Basin could act to weaken the atmospheric instability and intensify the anomalous sinking over the region, as well as to strengthen westerlies in the lower troposphere over the tropical Australian monsoon region and ascending flow over the eastern tropical Australian monsoon region. In turn, these changes result in strong TASM cases that favour enhanced summer rainfall in NEA. The opposite combination of factors is observed during the warm state of WB-SSTI.

The above results suggest that TASM strength is out of phase with SST anomalies over the Wharton Basin. A warmer-than-normal Wharton Basin SST favours a weak

TASM and corresponds to reduced summer rainfall in NEA, and vice versa. SST over the Wharton Basin has shown a continuous warming trend in the recent 60 years and has been in the warm state since the late 1970s (Figure 2(c)), when TASM entered a negative phase.

To further verify the above result on how the SST within WB influences the variations of TASM, we performed numerical experiments with CAM3 model. The control run was integrated for 15 years, which was used to derive a reference state. The sensitivity experiment was integrated for 17 years, the latter 15 years integrations were used to construct a 15-member ensemble mean to reduce the uncertainties arising from varying initial conditions. To isolate and mimic the impacts of SST variation, the only difference between the control and sensitivity experiment is 1°C decreasing in SST over Wharton Basin during summer. The associated differences between the sensitivity and control run are shown in Figure 8. It can be clearly seen that the cooling SST over Wharton Basin usually excites anomalous rising over NEA, favouring for more rainfall over NEA, which is consistent with the observation. This point supports the result that variation of Wharton Basin SST contributes to variations of TASM, in turn influences the variation of NEA summer rainfall. Therefore, we conclude that the warming of SST in the Wharton Basin is at least, in part, responsible for weakening of TASM, which in turn contributes to reduced rainfall over NEA.

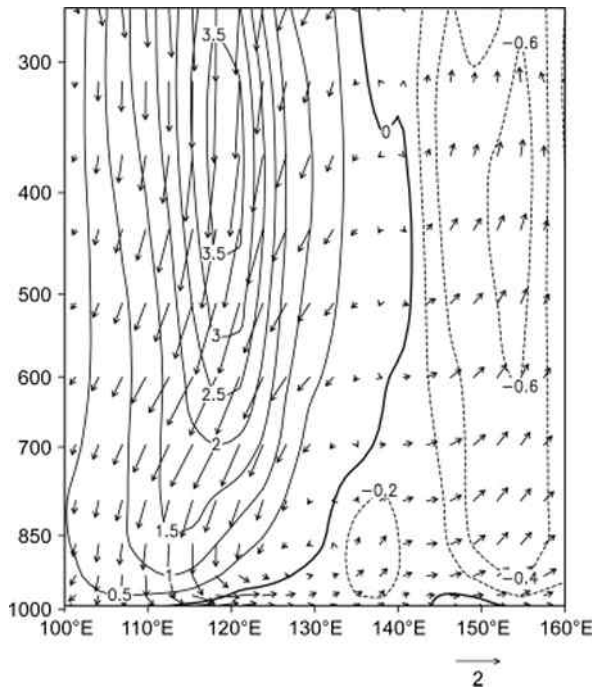


Figure 8. The zonal-height distribution of differences between sensitivity experiment with cooling SST over Wharton Basin and control run.

5. Discussion and conclusions

A remarkable feature of NEA summer rainfall is its long-term decreasing trend over the past 60 years. In this study, we analysed the possible cause of this decrease. First, NEA summer rainfall is associated with TASM. Variations in TASM capture not only interannual variability in NEA summer rainfall, but also interdecadal variations. In strong TASM years, enhanced rainfall over NEA is induced by strengthened westerlies over the tropical Australian monsoon region, a southward shift of ITCZ_NEA, enhanced cyclonic vorticity anomalies in the lower troposphere over eastern Australia and the adjacent ocean, enhanced rising over NEA, and enhanced water vapour transport over NEA; the opposite occurs during weak TASM years. TASM strength has shown a long-term weakening in the past 60 years and has been in a negative phase since the 1980s, when NEA summer rainfall entered a negative phase. Therefore, TASM weakening is responsible for the decrease in NEA summer rainfall.

Second, TASM is related to SST over the Wharton Basin. When the Wharton Basin SST is in a cold state, corresponding to increased convective stability, rising flow is suppressed over the basin. The associated reduction in dynamic instability over the tropical Australian monsoon region north to Australia, indicates anomalous easterlies in the high troposphere but strengthened westerlies in the lower troposphere. Consequently, TASM is intensified and convergence is enhanced over NEA.

Figure 9 shows a schematic of these processes that the potential influence of Wharton Basin SST has on TASM. SST in the Wharton Basin has shown a continuous

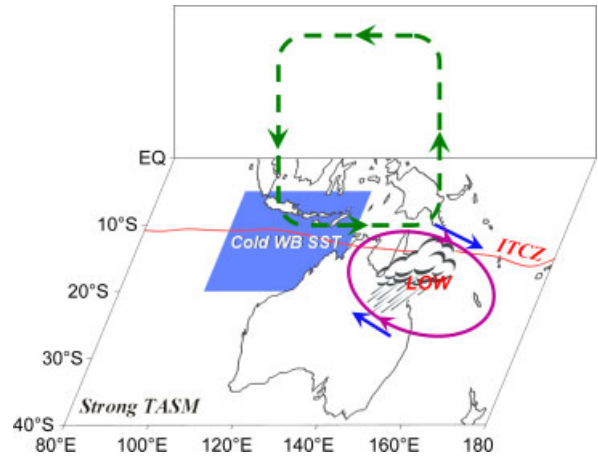


Figure 9. Schematic showing how TASM is related to Wharton Basin SST under a strong TASM state. This figure is available in colour online at wileyonlinelibrary.com/journal/joc

warming trend in recent decades, especially since the end of the 1970s, when it entered a long-term warm phase, coincident with a negative phase of TASM. This weakening in TASM is largely attributed to increasing SST in the Wharton Basin.

Independent of this study, Wang *et al.* (2004) defined an Australian summer monsoon index based on 850 hPa zonal wind anomalies averaged over the region (0° – 10° S, 120° – 150° E), following the traditional notion employed by Australian meteorologists. Hung and Yanai (2004) used the zonal wind at 850 hPa within the region (2° – 15° S, 115° – 150° E) to describe the characteristics of TASM. Their TASM indices are strongly correlated with that of the present study, yielding correlation coefficients of 0.85 and 0.94 (Figure 10(a), (b)), respectively. In addition, both indices show weakening trends and enter negative phases from the 1980s. This finding shows that the results of the present study are not dependent on the choice of TASM index.

The result in this study provides one of the possible causes for decline in rainfall over NEA, and indicates that the variations of SST within Wharton Basin contribute to the weakening of TASM. A very recent work of Cai *et al.* (2010) reported in association with a post-1980 positive phase of the interdecadal Pacific oscillation, the Walker circulation and convection center near Australia's east coast shift eastward, such that even during La Niña events, the convection center is still too far away from southeast Queensland, leading to a reduction in rainfall. One question rising is that whether the TASM is under influence of IPO, as well as the relationship of TASM and NEA summer rainfall, and what physical process is involved, these are all important questions and need further work.

Finally, TASM is a part of the Asian–Australian monsoon system, the relationship between the Asian and Australian monsoons has been discussed in several studies. Previous studies have reported that the East Asian winter monsoon (EAWM) shows strong interdecadal variability (Wu and Zhang 2006; Zhou *et al.*, 2007a, 2007b;

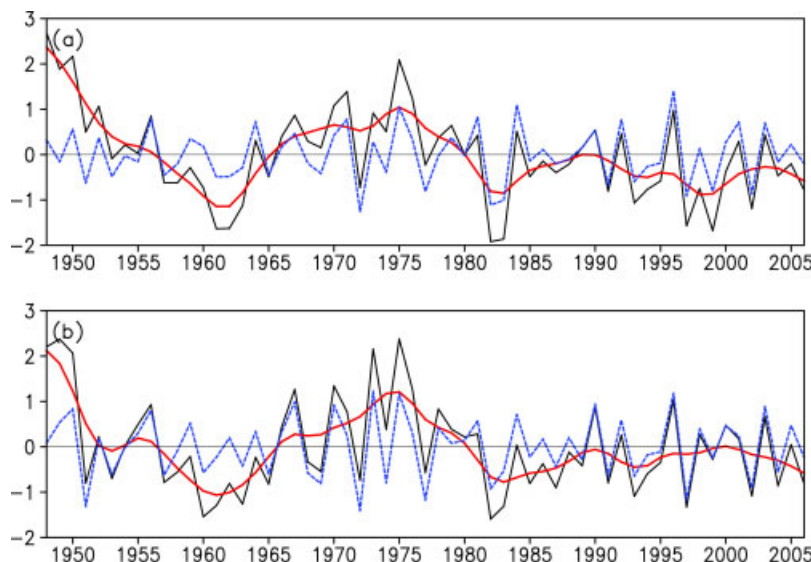


Figure 10. As in Figure 2, but for the normalized time series of (a) the TASM index defined by Wang *et al.* (2004) and (b) the TASM index defined by Hung and Yanai (2004). This figure is available in colour online at wileyonlinelibrary.com/journal/joc

Wu *et al.*, 2009). It is important to consider whether the EAWM influences rainfall variation over NEA. The regression pattern of TASMI with respect to geopotential height at 925 hPa (figure not shown) indicates that variations in TASM are linked to the strength of the Aleutian low, which is one of important reflections of EAWM variations (Nakamura *et al.*, 2002; Gao, 2007). The correlation coefficient between TASM and the Aleutian low index (defined as the areal mean SLP over the domain 40°–60°N, 150°E–140°W) is 0.42, significant at the 0.01 level. This result implies that variation in EAWM could influence the strength of TASM. This outcome raises the possible that variations in TASM are linked to EAWM, providing further support for the argument that EAWM contributes to variations in TASM. Therefore, topics for future work include the process and mechanism involved in the interaction between EAWM and TASM, and the relative contributions of EAWM to the weakening of TASM.

Acknowledgements

We thank the three anonymous referees whose comments greatly improved an earlier version of the manuscript. This work was jointly supported by the 973 Program (2010CB950400) and the Australia–China Bilateral Climate Change Partnerships Program of the Australian Department of Climate Change.

References

Ashok K, Guan ZY, Yamagata T. 2003. Influence of the Indian Ocean dipole on the Australian winter rainfall. *Geophysical Research Letter* **30**(15): 1821, DOI:10.1029/2003GL017926.

Cai WJ, Cowan T. 2006. SAM and regional rainfall in IPCC AR4 models: Can anthropogenic forcing account for southwest western Australian winter rainfall reduction? *Geophysical Research Letter* **33**: L24708, DOI:10.1029/2006GL028037.

Cai WJ, Cowan T, Sullivan A. 2009. Recent unprecedented skewness towards pIOD occurrences and its impacts on Australian rainfall. *Geophysical Research Letters* **36**: L11705, DOI:10.1029/2009GL037604.

Cai WJ, Rensch PV, Cowan T, *et al.* 2010. Asymmetry in ENSO teleconnection with regional rainfall, its multi-decadal variability, and impact. *Journal of Climate* **23**: 4944–4955.

Cai WJ, Shi G, Li Y. 2005. Multidecadal fluctuations of winter rainfall over southwest Western Australia simulated in the CSIRO Mark 3 coupled model. *Geophysical Research Letter* **32**: L12701, DOI:10.1029/2005GL022712.

Cai WJ, Watterson I. 2002. Modes of interannual variability of the Southern Hemisphere circulation simulated by the CSIRO climate model. *Journal of Climate* **15**: 1159–1174.

Cai WJ, Whetton PH, Pittock AB. 2001. Fluctuations of the relationship between ENSO and northeast Australian rainfall. *Climate Dynamics* **17**: 421–432.

Chen WY. 1982. Fluctuation in Northern Hemisphere 700 mb height field associated with the Southern Oscillation. *Monthly Weather Review* **110**: 808–823.

Davis RE. 1976. Predictability of sea-surface temperature and sea level pressure anomalies over the north Pacific Ocean. *Journal of Physical Oceanography* **6**: 249–266.

Drosdowsky W. 1993. An analysis of Australian seasonal rainfall anomalies: 1950–1987. II: Temporal variability and teleconnection patterns. *International Journal of Climatology* **13**: 111–149.

Drosdowsky W, Williams M. 1991. The Southern Oscillation in the Australian region. Part I: Anomalies at the extremes of the oscillation. *Journal of Climate* **4**: 619–638.

Feng J, Li JP. 2009. Variations of the South China Sea summer monsoon and its association with the global atmosphere circulation and sea surface temperature. *Chinese Journal of Atmospheric Sciences* **33**(3): 568–580.

Feng J, Li JP, Li Y. 2010a. A monsoon-like southwest Australian Circulation and its relation with rainfall in southwest Western Australia. *Journal of Climate* **23**: 1334–1653.

Feng J, Li JP, Li Y. 2010b. Is there a relationship between the SAM and southwest Western Australian winter rainfall? *Journal of Climate* **23**: 6082–6089.

Frederiksen CS, *et al.* 1999. Multidecadal simulations of Australian rainfall variability: the role of SSTs. *Journal of Climate* **12**: 357–379.

Gao H. 2007. Comparison of East Asian winter monsoon indices. *Advances in Geosciences* **10**: 31–37.

Hendon HH, Thompson DW, Wheeler MC. 2007. Australian rainfall and surface temperature variations associated with the Southern Hemisphere annular mode. *Journal of Climate* **20**: 2452–2467.

Hope P, Drosdowsky W, Nicholls N. 2006. Shifts in the synoptic systems influencing southwest Western Australia. *Climate Dynamics* **26**: 751–764.

Hung CW, Yanai M. 2004. Factors contributing to the onset of the Australian summer monsoon. *Quarterly Journal of the Royal Meteorological Society* **130**: 739–758.

IOCI. 2002. Climate variability and change in southwest Western Australia. Technical report, Indian Ocean Climate Initiative Panel, Perth; p. 34.

Kalnay EM, et al. 1996. The NCEP/NCAR reanalysis project. *Bulletin of the American Meteorological Society* **77**: 437–471.

Lau NC, Nath MJ. 1996. The role of the “atmospheric bridge” in linking tropical Pacific ENSO events to extratropical SST anomalies. *Journal of Climate* **9**: 2036–2057.

Li JP, Zeng QC. 2000. Significance of the normalized seasonality of wind field and its rationality for characterizing the monsoon. *Science in China (D)* **43**(6): 647–653.

Li JP, Zeng QC. 2002. A unified monsoon index. *Geophysical Research Letter* **29**(8): 1274, DOI:10.1029/2001GL013874.

Li JP, Zeng QC. 2003. A new monsoon index and the geographical distribution of the global monsoons. *Advances in Atmospheric Sciences* **20**: 299–302.

Li JP, Zeng QC. 2005. A new monsoon index, its interannual variability and relation with monsoon precipitation. *Climatic and Environmental Research* (in Chinese) **10**(3): 351–365.

Li Y, Cai WJ, Campbell EP. 2005. Statistical modeling of extreme rainfall in southwest Western Australia. *Journal of Climate* **18**: 852–863.

Meneghini B, Simmonds I, Smith IN. 2007. Association between Australian rainfall and the Southern Annular Mode. *International Journal of Climatology* **27**: 109–121.

McBride JL, Nicholls N. 1983. Seasonal relationships between Australian rainfall and the Southern Oscillation. *Monthly Weather Review* **111**: 1998–2004.

Murphy BF. 2004. Variability of southeast Queensland rainfall and its predictors. *International Journal of Climatology* **24**(6): 703–721.

Nakamura H, Izumi T, Sampe T. 2002. Interannual and decadal modulations recently observed in the Pacific storm track activity and East Asian winter monsoon. *Journal of Climate* **15**: 1855–1874.

Nicholls N. 1988. El Niño-Southern oscillation and rainfall variability. *Journal of Climate* **1**: 418–421.

Nicholls N. 1989. Sea surface temperatures and Australian winter rainfall. *Journal of Climate* **2**: 965–973.

Nicholls N. 2006. Detecting and attributing Australian climate change: a review. *Australian Meteorological Magazine* **55**: 199–211.

Nicholls N, Lavery B, Frederiksen C, et al. 1996. Recent apparent changes in relationships between the El Niño-Southern oscillation and Australian rainfall and temperature. *Geophysical Research Letter* **23**: 3357–3360.

Pitman AJ, Narisma GT, Pielke RA, et al. 2004. Impact of land cover change on the climate of southwest Western Australia. *Journal of Geophysical Research* **109**: D18109, DOI:10.1029/2003JD004347.

Power S, Casey T, Folland C, et al. 1999. Inter-decadal modulation of the impact of ENSO on Australia. *Climate Dynamics* **15**: 319–324.

Ropelewski CF. 1989. Precipitation patterns associated with high index phase of Southern Oscillation. *Journal of Climate* **2**: 268–284.

Ropelewski CF, Halpert MS. 1987. Global and regional scale precipitation patterns associated with El Niño/Southern Oscillation. *Monthly Weather Review* **115**: 1606–1626.

Rotstayan LD, Cai WJ, Martin RD, et al. 2006. Have Australian rainfall and cloudiness increased due to the remote effects of Asian Anthropogenic aerosols? *Journal of Geophysical Research* **112**: D09202, DOI:10.1029/2006JD007712.

Shi G, Cai WJ, Cowan T, et al. 2008a. Variability and trend over the northwest Western Australian rainfall: observations and coupled climate modeling. *Journal of Climate* **21**: 2938–2959.

Shi G, Ribble J, Cai WJ, et al. 2008b. An interpretation of Australian rainfall projections. *Geophysical Research Letters* **35**: L02702.

Simmonds I. 1990. A modeling study of winter circulation and precipitation anomalies associated with Australian region ocean temperature. *Australian Meteorological Magazine* **38**: 151–162.

Smith I. 2004. An assessment of recent trends in Australia rainfall. *Australian Meteorological Magazine* **53**: 163–173.

Smith IN, McIntosh P, Ansell TJ, et al. 2000. Southwestern Australian winter rainfall and its association with Indian Ocean climate variability. *International Journal of Climatology* **20**: 1913–1930.

Smith TM, Reynolds RW. 2004. Improved extended reconstruction of SST. (1854–1997). *Journal of Climate* **17**: 2466–2477.

Taschetto AS, England MH. 2008. An analysis of late 20th century trends in Australian rainfall. *International Journal of Climatology*, DOI:10.1002/joc.

Wang B, Kang IS, Lee JY. 2004. Ensemble simulations of Asian-Australian monsoon variability by 11 AGCMs. *Journal of Climate* **17**: 803–818.

Wardle R, Smith IN. 2004. Modeled response of the Australian monsoon to changes in land surface temperatures. *Geophysical Research Letters* **31**: L16205, DOI:10.1029/2004GL020157.

Wei DN, Sun JL, Li YP. 2008. Analysis of the anomalous strength and location of the ITCZ affecting the formation of northern Pacific typhoons. *Journal of Ocean University of China* **7**: 124–130.

Wu BY, Zhang RH. 2006. Distinct modes of the East Asian winter monsoon. *Journal of Climate* **134**: 2165–2179.

Wu ZW, Li JP, Wang B, Liu XH. 2009. Can the Southern Hemisphere annular mode affect China winter monsoon? *Journal of Geophysical Research* **114**: D11107, DOI:10.1029/2008JD011501.

Zhang L, Liao H, Li JP. 2010. Impact of the southeast Asian summer monsoon strength on the outflow of aerosols from South Asia. *Annales Geophysicae* **28**: 277–287.

Zhou W, Li CY, Wang X. 2007b. Possible connection between Pacific oceanic interdecadal pathway and East Asian winter monsoon. *Geophysical Research Letters* **34**: L01701, DOI:10.1029/2006GL027809.

Zhou W, Wang X, Zhou TJ, et al. 2007a. Interdecadal variability of the relationship between the East Asian winter monsoon and ENSO. *Meteorology and Atmospheric Physics* **98**: 283–293.